Optics Letters

Hyper-Rayleigh scattering in a strong coupling microcavity waveguide

Beiyi Zhang,[1] Hailang Dai,[1,3] and Xianfeng Chen[1,2,*]

[1]The State Key Laboratory on Fiber Optic Local Area Communication Networks and Advanced Optical Communication Systems, School of Physics and Astronomy, Shanghai JiaoTong University, Shanghai 200240, China
[2]Collaborative Innovation Center of Light Manipulations and Applications, Shandong Normal University, Jinan 250358, China
[3]e-mail: hailangdai@sjtu.edu.cn
*Corresponding author: xfchen@sjtu.edu.cn

Received 14 October 2020; revised 23 November 2020; accepted 8 December 2020; posted 17 December 2020 (Doc. ID 411384); published 25 January 2021

Second-harmonic generation (SHG) from hyper-Rayleigh scattering (HRS) in a hybrid strong coupling microcavity waveguide (HSCMW) was demonstrated, which indicates a possible method using continuous-wave (cw) incident light. The cw light was coupled into the waveguide with high coupling efficiency by free space coupling technology, and then the electric field intensity of the fundamental wave was enhanced due to local oscillation. HRS occurred by lithium niobite (LN) powder inside the waveguide, resulting in the direct observation of SHG in the transverse direction, with relatively high conversion efficiency measured to be 0.032%/W. This work suggests progress on frequency conversion and is also applicable to other nonlinear processes in a waveguide.

https://doi.org/10.1364/OL.411384

Second-harmonic generation (SHG) has found wide use in frequency conversion and makes hard-to-reach frequency domains more accessible. Many applications, such as bioimaging [1,2], quantum information [3], optical switching [4], and surface magnetism [5], can be realized through SHG. In general, efficient SHG requires the phase-matching (PM) condition, which is usually obtained through the birefringent crystal. However, the PM condition limits the wavelength region and polarizing angle of SHG processes strictly. In order to achieve SHG in a broad bandwidth, quasi-phase-matching (QPM) [6] and metasurfaces [7] are proposed. The QPM can be applied because the optical axis of poled material has a periodical alternation in orientation, which provides a reversed periodically susceptibility to compensate the phase mismatching. By modifying the grating period to satisfy wave vector matching, efficient SHG can be achieved [8–11]. Alternatively, the metasurface which consists of metallic and dielectric nanostructures is another option. For applications, researchers prefer to control the geometry and chemical composition of "artificial atoms" within a very thin metasurface to control the phase, amplitude, and polarization of light that is transmitted, reflected, or scattered, rather than the traditional method of controlling light on the propagation path. The metasurface can provide a new degree of freedom to control the wavefront [12–14]. However, due to some basic shortcomings with the traditional way to SHG, the current application is still limited. For example, the excessive power of the fundamental frequency wave (FW) will cause crystal breakdown, and SHG also suffers from low efficiency [8], which hinders practical application. Actually, the direct observation of localized SHG in metal nanostructures has been reported [15–17] which relaxes the stringent phase-matching condition, providing a way to enhance SHG by a metal nanostructure or material. The efficiency of the frequency conversion is proportional to the intensity of the FW [18], so it is possible to realize SHG through the FW localization. The hyper-Rayleigh scattering (HRS) in a solution provides a method to determine the hyperpolarization of nonlinear molecules via SHG scattering light [19]. In the theory of HRS, the power of SHG is proportional to the 4th power of the electric field [20]. Therefore, it can be inferred that the highly efficient SHG from HRS can be achieved in the strong electric field of FW.

In this Letter, we present a type of hybrid strong coupling microcavity waveguide (HSCMW) [21] to achieve a strong enhancement of the electric field of the FW (E_{FW}), and efficient SHG can be realized from HRS. The HSCMW excites ultrahigh-order modes (UOMs) and localizes energy of the FW in a capillary [21]. Hence, the superfine lithium niobite (LN) particles in the suspension injected into the capillary of the HSCMW are induced to generate 2nd-order polarization and generate efficient SHG during the HRS process in the capillary. The SHG light beam can be directly visualized utilizing the HSCMW structure with low-power continuous-wave (cw) incidence. Within the electric dipole approximation, the action of a single scattering particle is described by the hyperpolarizability.

We start with a description on the physical picture of the SHG process in our experiments by theoretical analysis. When FW incidents on capillary, the particle experiences two different scatterings simultaneously. As Fig. 1(a) shows, one is linear Rayleigh scattering (RS) with the same frequency as FW (marked in red), and the other is 2nd-order nonlinear HRS with double frequency (marked in green), which is the source of SHG. Every polarized particle radiates SHG, and the total detected SHG is their incoherent superposition. For further understanding the physics behind the analysis mentioned above, we numerically

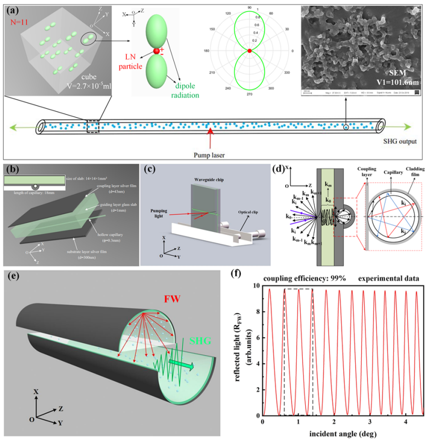

Fig. 1. (a) Principle of SHG from HRS. Inset: the LN powder as scattering particles of which the average diameter is around 100 nm under SEM. (b) Structure of HSCMW. (c) 1064 nm cw incidents nearly vertical and generating the SHG horizontally. (d) Distribution of E. (e) High energy density field and dense particles increase the intensity of SHG. (f) Attenuated total reflectance (ATR) peaks detected, representing reflected intensity of the modes with scan at incident angle.

calculated the intensity of SHG (I_{SHG}). Based on the theory of nonlinear optics, the relationship between the electric field (E) and the light intensity (I) is $I = 2n\sqrt{\varepsilon_0/\mu_0}|\vec{E}|^2$ [22]. According to the theory of electric dipole radiation [23], the polarization (P) from one particle can be obtained,

$$p = \varepsilon_0 \chi^{(2)} E_{\mathrm{FW}}^2, \quad \vec{P} = V\vec{p}, \tag{1}$$

where E_{FW} is the electric field of FW, V is the volume of a particle, and $\chi^{(2)}$ is the nonlinear susceptibility of LN.

Then the electric field of SHG (E_{SHG}) can be derived from P and finally a simple formula of I_{SHG} from one particle can be obtained:

$$\vec{E}_{\mathrm{SHG}} = \frac{1}{4\pi\varepsilon_0 c^2 R}\left|\ddot{\vec{P}}\right| e^{ikR}\sin\theta\,\vec{e}_\theta, \tag{2}$$

$$I = 2n\sqrt{\frac{\varepsilon_0}{\mu_0}}\left|\vec{E}_{\mathrm{SHG}}\right|^2 = 2n\sqrt{\frac{\varepsilon_0}{\mu_0}}\frac{\omega^4}{\pi^2{\varepsilon_0}^2 c^4 R^2}(pV)^2\sin^2\theta, \tag{3}$$

$$\text{power} = \int_0^{\pi}\int_0^{\pi} 2Ir\sin\theta\,\mathrm{d}\varphi r\,\mathrm{d}\theta, \tag{4}$$

$$I_{\mathrm{SHG}} = \frac{\text{power}}{S} = \frac{16}{3}n\sqrt{\frac{\varepsilon_0}{\mu_0}}\frac{\omega^4\left(\varepsilon_0\chi^{(2)}V\right)^2}{\pi{\varepsilon_0}^2 c^4 S}E_{\mathrm{FW}}^4, \tag{5}$$

where ω and k are the angular frequency and wave vector of the FW, respectively, and S is the cross-section area of the capillary. For details of the theoretical calculation, see Supplement 1.

Notably, there is an obvious consequence:

$$I_{\mathrm{SHG}} = \mathrm{A}\frac{D^6}{\lambda^4}d^2 E_{\mathrm{FW}}^4, \quad \mathrm{A} = \frac{256}{27}n\sqrt{\frac{\varepsilon_0}{\mu_0}}\frac{\pi^5}{S}, \tag{6}$$

where D is the diameter of particle, d is the nonlinear coefficient, and $d = 1/2\chi$. A is a constant coefficient depending on S. Finally, the intensity of SHG from all particles (I_{ALL}) can be deduced by using the incoherent superposition theory:

$$I_{\mathrm{ALL}} = I_{\mathrm{SHG}} \times N = \mathrm{A}ND^6 d^2 E^4/\lambda^4, \tag{7}$$

where N is the number of LN particles in the capillary. Equation (7) indicates that high I_{SHG} can be obtained by enhancing the electric field of the FW.

As we calculated above, I_{SHG} is proportional to the 4th power of E_{FW} : $I_{\mathrm{SHG}} \propto E_{\mathrm{FW}}^4$. Thus, the HSCMW is proposed aiming to enhance E_{FW} greatly. As shown in Fig. 1(b), the HSCMW comprises a slab metal-cladded waveguide (14 × 14 × 1 mm) and a hollow-core capillary with a 0.3 mm internal diameter and an 18 mm length. The metal-cladded waveguide includes a thin silver film as the coupling layer (43 nm thick) on the top, a glass slab as the guiding layer (1 mm thick) in the middle with a hollow capillary together, and a thicker silver film as the substrate layer (300 nm thick) at the bottom. The parallelism of the upper and lower surfaces of the glass slab is less than 4″. As Fig. 1(c) shows, when the incident light (1064 nm, 30 mW, cw, FWHM is 0.56 nm) irradiates on the top of the structure at a very small incident angle (θ), which matches with the coupling angle, the incident light can be coupled into the waveguide layer of HSCMW by resonating with the eigenmode of the cavity, emphasizing that the waveguide layer includes a slab glass and hollow-core capillary. Then the UOMs [21] will be excited under the matching condition by free-space coupling technology [24], resulting in a high-density power standing wave field localized in the capillary, as shown in Fig. 1(d). Because the UOMs' standing wave field oscillates between the top and bottom layer at a very small incident angle [25], there are many unique features of the UOMs, such as high sensitivity, high power density, and high quality factor, compared to low-order modes like the surface plasmon polaritons mode.

The UOMs propagate in the y direction and induce a standing wave field in the z direction. When the LN powder suspension is injected into the hollow-core capillary, the high energy density oscillating field generates strong HRS which generates a second-harmonic wave. Moreover, the SHG accumulates through the incoherent superposition in the y direction, as shown in Fig. 1(e). At the coupling point, the SHG is weak initially in the middle of the capillary and enhances with the increase of the propagating distance because of the continuous accumulation from every particle. Ultimately, the generated SHG can be visualized at the end of capillary.

In our HSCMW, the enhancement of E_{FW} can be explained by two facts. First, E_{FW} in the guiding layer is enhanced by 8 times that in the air before coupling into the slab metal-cladded waveguide [26]. Then the energy of the UOMs excited in the guiding layer can be coupled into the capillary almost 100%, because the coupling efficiency is quite large; this is inversely proportional to the effective refractive index [27], see Supplement 1. To draw an analogy, the FW is enhanced by 8 times from the air to the guiding layer, because of a one-dimensional constraint in the guiding layer on E_{FW} and the high coupling efficiency. As a result, we can infer that the UOMs are enhanced in the same way from the guiding layer to the capillary because of the two-dimensional constraints in the capillary and the high coupling efficiency. Therefore, E_{FW} in the capillary is approximately enhanced by 64 times that in the air before coupling, which means we can obtain relatively high I_{SHG} in our HSCMW by cw FW incidence theoretically. The measured coupling efficiency of our microwaveguide from the

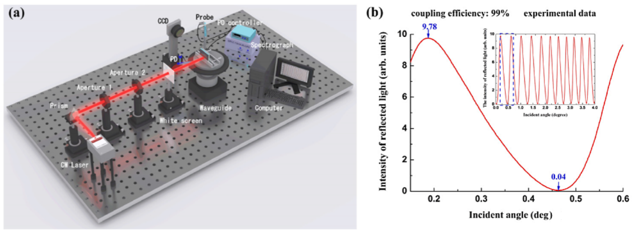

Fig. 2. (a) Experiment systems and equipment. (b) Coupling efficiency of FW is equal to ~0.9959.

air to the capillary is higher than 99%, owing to mature coating technology, as shown in Figs. 1(f) and 2(b).

In our experiment, the value of quality factor $Q \sim 10^4$ by measurement [21]. According to the theory of cavity Q [28], I_{FW} in the guiding layer is enhanced by 66 times that in air before coupling into the slab metal-cladded waveguide, which is extremely close to the theoretical valuation 64 times, see Supplement 1.

In Fig. 2(a), a computer-controlled $\theta/2\theta$ goniometer is applied for the accurate angular scanning of the incidence to ensure efficient energy coupling. The spectrograph (*Andor Shamrock 500i*) and photoelectric detector (PD) are used to detect the spectroscopy and intensity of the SHG, respectively.

LN is an artificial synthetic material with excellent nonlinear performance and a high refractive index ($n \approx 2.2$). In our experiments, we use the superfine LN powder as the scattering medium, which is prepared by the crystal growth method using niobium pentoxide (Nb_2O_5) and lithium acetate dihydrate ($C_2H_3O_2Li{\cdot}2H_2O$) as the reactants, ground into powder, and then suspended in absolute ethyl alcohol (99.5%). The average diameter of LN powder particles is ~100 nm under a scanning electron microscope (SEM), as shown in the rightmost part of Fig. 1(a). The concentrations of the LN powder suspension are from 10^{-5} to 10^{-14} g/ml. The LN suspension is injected into the hollow-core capillary using a microsyringe. To avoid the LN particles depositing, it is necessary to vibrate in an ultrasonic machine before injection.

The SHG green spot which can be directly visualized and its spectroscopy are shown in Fig. 3(a). As Figs. 3(b)–3(e) show, the SHG beam increases gradually along the capillary in four images, which are captured from experimental video at different times. The video shows that the SHG beam keeps relative stability all the time when the FW illuminating. There is a small fluctuation due to Brownian movement and the instability of the pump light. Meanwhile, the spectrograph and power meter detect the average power of the SHG.

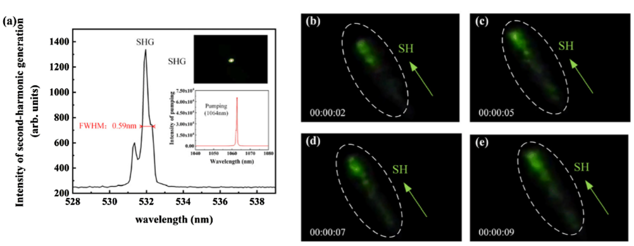

Fig. 3. Experimental detected spectrum and SHG light. (a) Accurate incident FW central wavelength is ~1064 nm, and the central wavelength of SHG is ~532 nm. (b)–(e) Captured four images at different times from experimental video (see Visualization 1).

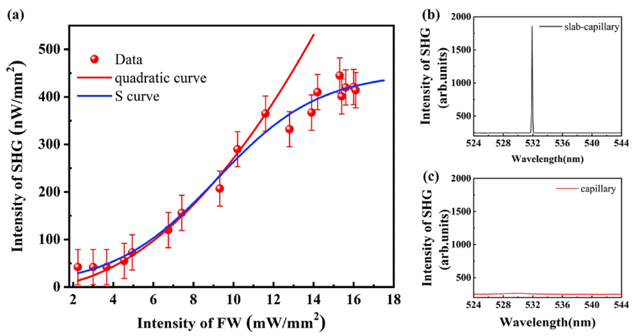

Fig. 4. (a) Intensity of SHG emitted by LN powder versus the excitation intensity of FW. (b) Large SHG peak is observed demonstrating the superiority of the HSCMW. (c) Only noise is observed.

Figure 4(a) shows the emission SHG intensity as a function of the excitation FW intensity. The cw FW intensity is from 2 to 16 $\mathrm{mW/mm^2}$, and the generated SHG intensity is from 0.1 to 0.45 $\mu\mathrm{W/mm^2}$. According to the theory we had before, the functional relationship of I_{FW} and I_{SHG} is quadratic. Therefore a quadratic function is used to fit the experiment data with the expression of $I_{SHG} = A I_{FW}^2$ (marked in red), where A is a constant coefficient. As the fitted curve shows, it can give a good description for the situation of a lower I_{FW}. However, when I_{FW} increases, I_{SHG} reaches saturation gradually, so we use another fitted curve S curve (marked in blue) to describe the general trend. The observation results of our experiment showed different I_{SHG} with different concentrations of LN suspension. We found when the concentration of LN suspension increases, I_{SHG} shows a Gaussian-like distribution, and the highest I_{SHG} peak appears at the concentration of 10^{-10} g/ml, see Supplement 1. There is a reasonable explanation for the phenomenon: a competition between scattering and cluster exists in LN particle suspension [29]. When the LN particles absorb heat under a higher I_{FW}, the Brownian motion among particles will intensify which increases the chance of particle collisions. The 100 nm particles form clusters easier at the higher probability of collisions, and then Mie scattering or geometric scattering will be more suitable instead of HRS [23]. That is why I_{SHG} reaches saturation gradually. It is the same situation when the concentration of the suspension changes. At a low LN concentration, the low probability of cluster due to rare collisions among particles results in high I_{SHG}, and as the concentration increases collisions aggravate leading to more clusters which hinders SHG. Moreover, the conversion efficiency of SHG $\gamma = P_{SHG}/P_{FW}$ can be calculated by the experimental data measured, where P_{SHG} and P_{FW} are the power of the SHG and FW, respectively. As shown in Fig. 4(a), we can achieve the conversion efficiency of SHG $\gamma = (37\ \mathrm{nW}/11.6\ \mathrm{mW}) \times 100\% = 3.2 \times 10^{-4}\%$, which means the normalized conversion efficiency of SHG $\gamma = 0.032\%/\mathrm{W}$ if the power of the FW is 1 W.

To verify the unique features of the UOMs and the HSCMW, a comparison experiment has been presented in Figs. 4(b) and 4(c). One is hollow-core capillary only, and another is the HSCMW. Only noise is observed for the capillary structure without any signal peak detected as shown in Fig. 4(c), which demonstrates forcefully the superior performance of our HSCMW.

Substituting the experimental results into Eq. (7), we find the theoretical result showing good agreements with the experimental result. A set of experimental data from Fig. 4(a) is chosen: $I_{\mathrm{FW}} = 11.6\,\mathrm{mW/mm^2}$, $I_{\mathrm{SHG}} = 370\,\mathrm{nW/mm^2}$, and $N = 1046$ for the concentration of 10^{-9} g/ml, see Supplement 1. If we calculate I_{ALL} using E_{FW} of the experimental incident light, $I_{\mathrm{ALL}} = 3.68 \times 10^{-8}\,\mathrm{W/m^2}$. Actually, E_{FW} in the capillary is enhanced by 64 times that in air before coupling, which has been discussed above, resulting in the theoretical value $I'_{\mathrm{ALL}} = 0.617\,\mathrm{W/m^2}$. In our experiments, the experimental value we detected is $0.370\,\mathrm{W/m^2}$. Unavoidably, there are some experimental errors such as absorption and loss which makes the theoretical result bigger than the calculation result. According to Eq. (7), we can obtain the relationship between effective nonlinear coefficient d_{eff} and theoretical nonlinear coefficient d: $0.617/34.45^2 = 0.307/d_{\mathrm{eff}}^2$, where $0.370\,\mathrm{W/m^2}$ and $0.617\,\mathrm{W/m^2}$ are the experimental value and the theoretical value obtained above, respectively. We can deduce $d_{\mathrm{eff}} = 24.30\,\mathrm{pmV^{-1}}$, and the value is between $d_{33} = 34.45\,\mathrm{pmV^{-1}}$ and $d_{22} = 3.07\,\mathrm{pmV^{-1}}$ [22] because of the anisotropy of LN.

In conclusion, we have theoretically analyzed and experimentally demonstrated the efficient SHG occurred in a HSCMW through HRS by LN particles. We achieve the normalized conversion efficiency of SHG by a cw FW. The experimental data demonstrate that our design is a significant progress on nonlinear frequency conversion. SHG combining HRS with a HSCMW vastly simplifies the machining process and complex structure compared to the traditional way to SHG. Also, it shows a potential approach in nonlinear frequency conversion with relatively high conversion efficiency. For further research, we will consider the chemical surface modification on particles which can prevent particles from clustering to obtain higher conversion efficiency.

Funding. National Key Research and Development Program of China (2017YFA0303701, 2018YFA0306301); National Natural Science Foundation of China (11734011, 11764020, 11974245); Foundation for Development of Science and Technology of Shanghai (17JC1400400); Shanghai Municipal Science and Technology Major Project (2019SHZDZX01).

Acknowledgment. The author thanks Prof. Xianfeng Chen for the helpful discussion and Hailang Dai for help in the experimental design and laboratory.

Disclosures. The authors declare no conflicts of interest.

Supplemental document. See Supplement 1 for supporting content.

REFERENCES

1. P. J. Campagnola and L. M. Loew, Nat. Biotechnol. **21**, 1356 (2003).
2. Z. Tang, D. King, and S. Liu, Science **47**, 8 (2004).
3. V. G. Avramenko and T. V. Dolgova, Phys. Rev. B **73**, 155321 (2006).
4. Y. Okada, S. Matsumoto, Y. Takanishi, K. Ishikawa, S. Nakahara, K. Kishikawa, and H. Takezoe, Phys. Rev. E **72**, 020701 (2005).
5. J. Reif, J. C. Zink, C.-M. Schneider, and J. Kirschner, Phys. Rev. Lett. **67**, 2878 (1991).
6. P. Xu, S. H. Ji, S. N. Zhu, X. Q. Yu, J. Sun, H. T. Wang, J. L. He, Y. Y. Zhu, and N. B. Ming, Phys. Rev. Lett. **93**, 133904 (2004).
7. C. G. Biris and N. C. Panoiu, Phys. Rev. B **81**, 195102 (2010).
8. B. Chen, C. Zhang, C. Hu, R. Liu, and Z. Li, Phys. Rev. Lett. **115**, 083902 (2015).
9. D. T. Reid, J. Opt. A **5**, S97 (2003).
10. X. Chen, P. Karpinski, V. Shvedov, A. Boes, A. Mitchell, W. Krolikowski, and Y. Sheng, Opt. Lett. **41**, 2410 (2016).
11. T. Xu, D. Lu, H. Yu, H. Zhang, Y. Zhang, and J. Wang, Appl. Phys. Lett. **108**, 051907 (2016).
12. A. V. Kildishev, A. Boltasseva, and V. M. Shalaev, Science **339**, 1232009 (2013).
13. J. Qin, F. Huang, and X. Li, ACS Nano **13**, 10768 (2019).
14. D. Lin, P. Fan, E. Hasman, and M. L. Brongersma, Science **345**, 298 (2014).
15. S. I. Bozhevolnyi, J. Beerman, and V. Coello, Phys. Rev. Lett. **90**, 197403 (2003).
16. Z. Hu, Q. Zhang, and B. Miao, Phys. Rev. Lett. **109**, 253901 (2012).
17. S. K. Turitsyn, S. A. Babin, and A. E. El-Taher, Nat. Photonics **4**, 231 (2010).
18. A. M. Weiner, A. M. Kan'an, and D. E. Leaird, Opt. Lett. **23**, 1441 (1998).
19. K. Clays and A. Persoons, Phys. Rev. Lett. **66**, 2980 (1991).
20. K. Clays, E. Hendrickx, and M. Triest, J. Mol. Liq. **67**, 133 (1995).
21. H. Dai, C. Yin, Z. Xiao, Z. Cao, and X. Chen, Phys. Rev. Appl. **11**, 064055 (2019).
22. R. Boyd, *Nonlinear Optics* (Academic, 2019).
23. J. Jackson, *Classical Electrodynamics* (Wiley, 2007).
24. H. Li, Z. Cao, H. Lu, and Q. Shen, Appl. Phys. Lett. **83**, 2757 (2003).
25. L. Chen, Z. Cao, and F. Ou, Opt. Lett. **32**, 1432 (2007).
26. W. Yuan, C. Yin, and P. Xiao, Microfluid. Nanofluid. **11**, 781 (2011).
27. Y. Zheng, W. Yuan, and X. Chen, *Conference on Lasers and Electro-Optics* (2012), paper JW4A.1.
28. K. J. Vahala, Nature **424**, 839 (2003).
29. J. Lakowicz, *Principles of Fluorescence Spectroscopy* (Springer, 2013).